J. Chem. Sci., Vol. 118, No. 1, January 2006, pp. 15–21.

Influence of fuel ratios on auto combustion synthesis of barium ferrite nano particles

D BAHADUR*, S RAJAKUMAR and ANKIT KUMAR

Department of Metallurgical Engineering and Materials Science, Indian Institute of Technology, Mumbai 400 076
e-mail: dhirenb@iitb.ac.in

Abstract. Single-domain barium ferrite nano particles have been synthesized with narrow particle-size distribution using an auto combustion technique. In this process, citric acid was used as a fuel. Ratios of cation to fuel were maintained variously at 1 : 1, 1 : 2 and 1 : 3. The pH was 7 in all cases. Of all three cases, a cation to citric acid ratio of 1 : 2 gives better yield in the formation of crystalline and single domain particles with a narrow range of size distribution. Most particles are in the range of 80 to 100 nm. Maximum magnetization and coercivity values are also greater for 1 : 2 ratios. These values measured at room temperature are found to be 55 emu/gram and 5000 Oe respectively. XPS and ESR studies support the results.

Keywords. Nano particle synthesis; autocombustion; fuel ratios; barium ferrite.

1. Introduction

Nano-sized barium ferrite with hexagonal molecular structure ($BaFe_{12}O_{19}$) is a known high performance permanent magnetic material.[1] owing to its fairly large magneto crystalline anisotropy, high Curie temperature, and relatively large magnetization, as well as its excellent chemical stability and corrosion resistivity. For ideal performance, barium ferrite particles are required to be of single magnetic domain, good chemical homogeneity and narrow particle-size distribution. The interest in these nano-sized particles lies in our ability to affect their physical properties through manipulation of size, composition and aspect ratio to produce changes in overall physical properties.

Recent studies have shown that physical properties of nano particles are influenced significantly by the processing techniques.[2] Since crystallite size, distribution of particle sizes and inter particle spacing have the greatest impact on magnetic properties, the ideal synthesis technique must provide superior control over these parameters.[3] A variety of techniques has been employed for the synthesis of nano particles with definite shapes and sizes.[4–6]

Self-propagating high temperature synthesis (SHS) also known as auto combustion is an important technique widely used for the synthesis of a variety of oxides for different applications.[7–10] Synthesis of hard ferrites has been reported by using the sol–gel auto combustion technique.[11] This combustion method presents some advantages over other methods: the reagents are simple compounds, special equipment is not required (Pyrex containers are used), dopants can be easily introduced into the final product, and agglomeration of powders remains limited. The method uses the energy produced by the exothermic decomposition of a redox mixture of metal nitrates with an organic compound. In the combustion mixture, nitrates and organic compounds behave like conventional oxidants and fuels. The reaction is carried out by dissolving metal nitrates and fuels in a minimum amount of water in a pyrex dish and heating the mixture in order to evaporate water in excess. The resulting viscous liquid foams, ignites, and undergoes self-sustained combustion, producing ashes containing the oxide product. During the combustion, exothermic redox reactions associated with nitrate decomposition and fuel oxidation take place. Gases such as N_2, H_2O, and CO_2 evolve, favouring the formation of fine particle ashes after only a few minutes. The properties of the final product (particle size, surface area and porosity) depend on the method of combustion. The departure of gases favours the desegregation of the products (increases the porosity) and heat dissipation (inhibits the sintering of the pro-

Dedicated to Prof J Gopalakrishnan on his 62nd birthday
*For correspondence

ducts). Exothermicity of combustion is controlled by the nature of the fuel and the ratio of oxidizer to fuel. The reaction paths for the synthesis have been described elsewhere.[12]

The combustion synthesis is also advantageous over the solid state synthesis in terms of better compositional homogeneity and purity of the final product.[13] However, only a few efforts have been made to correlate the effect of synthesis parameters like pH,[14] fuel-to-oxidant ratio,[15] and effect of different fuels[16] with powder characteristics. Here, an effort has been made to identify the effect of fuel ratios on barium ferrite synthesis at a lower pH value of 7 and their influence on size, morphology and magnetic properties.

2. Experimental procedure

For the preparation of barium ferrite nano particles, analytical grade barium nitrate $Ba(NO_3)_2$ of purity 99·5%, AR grade ferric nitrate $Fe(NO_3)_3{\cdot}9H_2O$ of 98% purity and AR grade citric acid of 99·5% were taken as starting materials. Although the stoichiometric Fe/Ba ratio should be 12 for $BaFe_{12}O_{19}$, it was reported that an excess of barium is needed to ensure the formation of single-phase $BaFe_{12}O_{19}$.[17,18] Affleck *et al*[19] suggested that a small amount of barium volatilizes during the combustion and calcinations process, which is responsible for the "off stoichiometry". Huang *et al*[20] have tried different ratios of Ba/Fe and established that a ratio of 1 : 11·5 gives single-phase ferrites. Hence, the molar ratio of Ba to Fe was fixed at 1 : 11·5. The nitrates were dissolved with a minimum amount of de-ionized water to get a clear solution. Three samples with different fuel ratios were prepared as follows.

(a) Bf11 – cations: citric acid = 1 : 1
(b) Bf12 – cations: citric acid = 1 : 2
(c) Bf13 – cations: citric acid = 1 : 3.

An aqueous solution of citric acid was mixed with the nitrate solution in the required ratio. After complete dissolution of all starting materials, an appropriate amount of nitric acid/ammonia solution was added dropwise to this solution with constant stirring until the pH reached 7. The resulting solution was then heated on a hot plate, whose temperature was maintained around 80° to 90°C. This process was continued for 3 to 4 hours, after which the transparent solution turned to viscous brown gel followed by foaming of the gel. The foamy gel was kept on a pre-heated oven at 150°C which caused its spontaneous ignition. The combustion reaction was completed within a few seconds and loose powder was formed. This was crushed and ground thoroughly. The fine powder sample was then heat-treated at 450°C for 24 h to remove carboneous materials and at 850°C for 6 h for the final formation of barium ferrite nano particles.

To confirm the formation of a single phase, X-ray diffraction analyses of the synthesized powdered samples were done between 20° and 90° angle using a PANalytical XPERT-PRO diffractometer with CuK_a radiation. Particle size and morphology of the samples were examined by Philips C200 transmission electron microscope (TEM) operated at 200 kV. Magnetic properties of the hexaferrite samples were measured by using a vibrating sample magnetometer with a maximum applied field of 20 kOe. Room temperature electron spin resonance (ESR) spectra of the samples were recorded on an X-band (9·11 GHz) Elinc Century Series EPR spectrometer. Electronic spectroscopy for chemical analysis (ESCA) was also performed on a Thermo VG Scientific Multilab 2000 instrument using a 15 kV Al K-*a* gun.

3. Results and discussion

The as-prepared samples consist of oxide and carboneous forms of the starting constituents. The samples are then calcined in a two-stage heat treatment process, 430°C for 24 h and 850°C for 6 h for the removal of impurities to get nano particles of single-phase

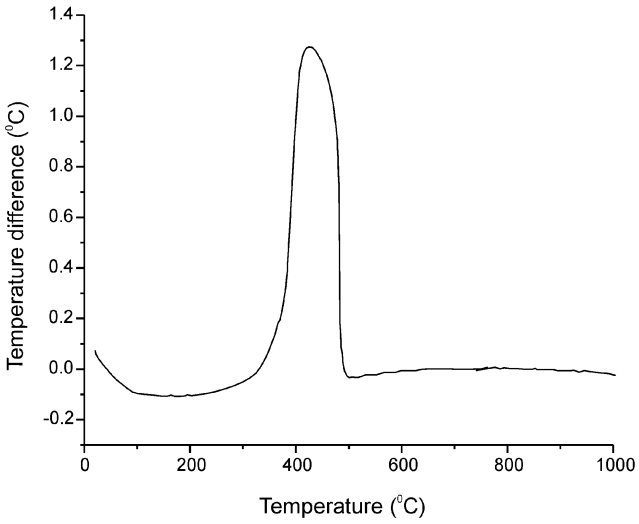

Figure 1. Differential thermal analysis of BfC11.

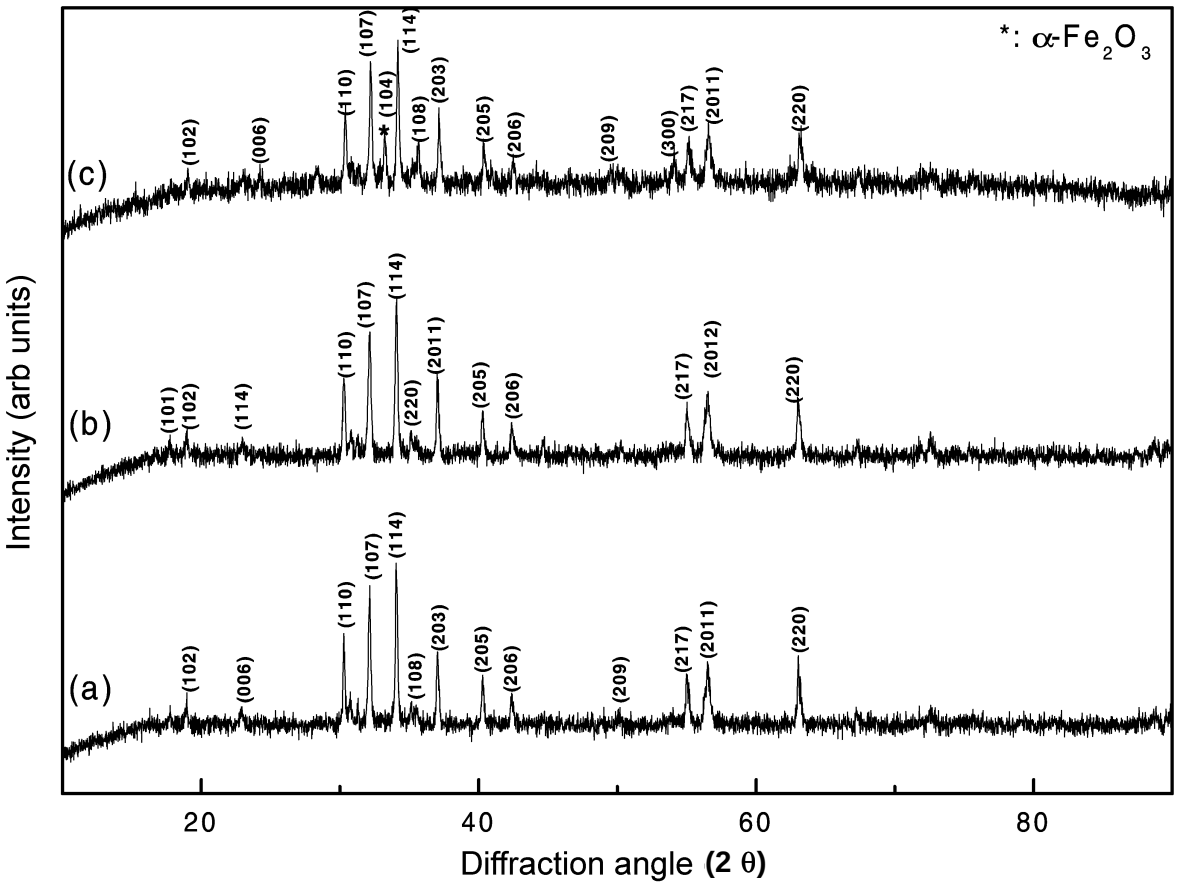

Figure 2. XRD patterns of the samples heat-treated at 450°C for 24 h and 850°C for 6 h. Samples are (**a**) Bf11, (**b**) Bf12 and (**c**) Bf13.

barium ferrite. The temperature for the first stage of heat treatment is estimated from the DTA curve of the sample as shown in figure 1.

The X-ray diffraction patterns of the samples are shown in figure 2 which match exactly with the standard powder diffraction file no. 07-0276, 84-0757, confirming the formation of single-phase barium ferrite particles. However, at higher fuel ratio 1 : 3, there are some traces of iron oxide peaks. The single phase may also have been promoted due to calcinations of samples at 850°C for longer time durations.

The XPS data for the sample BfC12 as a typical example is presented in figure 3. The binding energies are determined from the C_{1s} peak at 287 eV. The Ba $^3d_{5/2}$ and Ba $^3d_{3/2}$ peaks are observed at 782·1 and 797·5 eV respectively, and the Fe $^2p_{3/2}$ and Fe $^2p_{1/2}$ peaks are seen at 713·47 and 726·89 eV respectively, which are characteristic of the sample.[21] The small shift in binding energy of the Ba peak in ferrite as compared to that in BaO is due to the different environments in which the Ba ion is placed in the two compounds, which contribute to the difference in relaxation effect.

In the ferrite, the presence of $Fe_{3þ}$ is detected and confirmed by its distinct characteristic satellite peak at around 8·0 eV above the principal peak. The observation of a distinct satellite at 8·0 eV above the main peak indicates the absence of Fe_3O_4 phase in the material. Fe_3O_4 does not show any satellite[22] due to overlapping of the satellite peaks for Fe^{3+} (at a separation of 8·0 eV) and Fe^{2+} (at a separation of 6·0 eV) resulting in the formation of a broad background. Usually $^2p_{3/2}$ binding energy is in the range 711–711·4 eV with a satellite-primary peak energy separation of about 8·5 eV. According to Allen and co-workers,[23,24] such binding energy concerns materials in which the $Fe_{3þ}$ concentration is higher than that of $Fe_{2þ}$. The large values of FWHM show that the iron distribution is complex. The binding energy of the O 1*s* peak is about 532 eV. This energy is in agreement with results from the literature.[24] The O 1*s* spectrum shows a large FWHM of approx 1·8 eV.

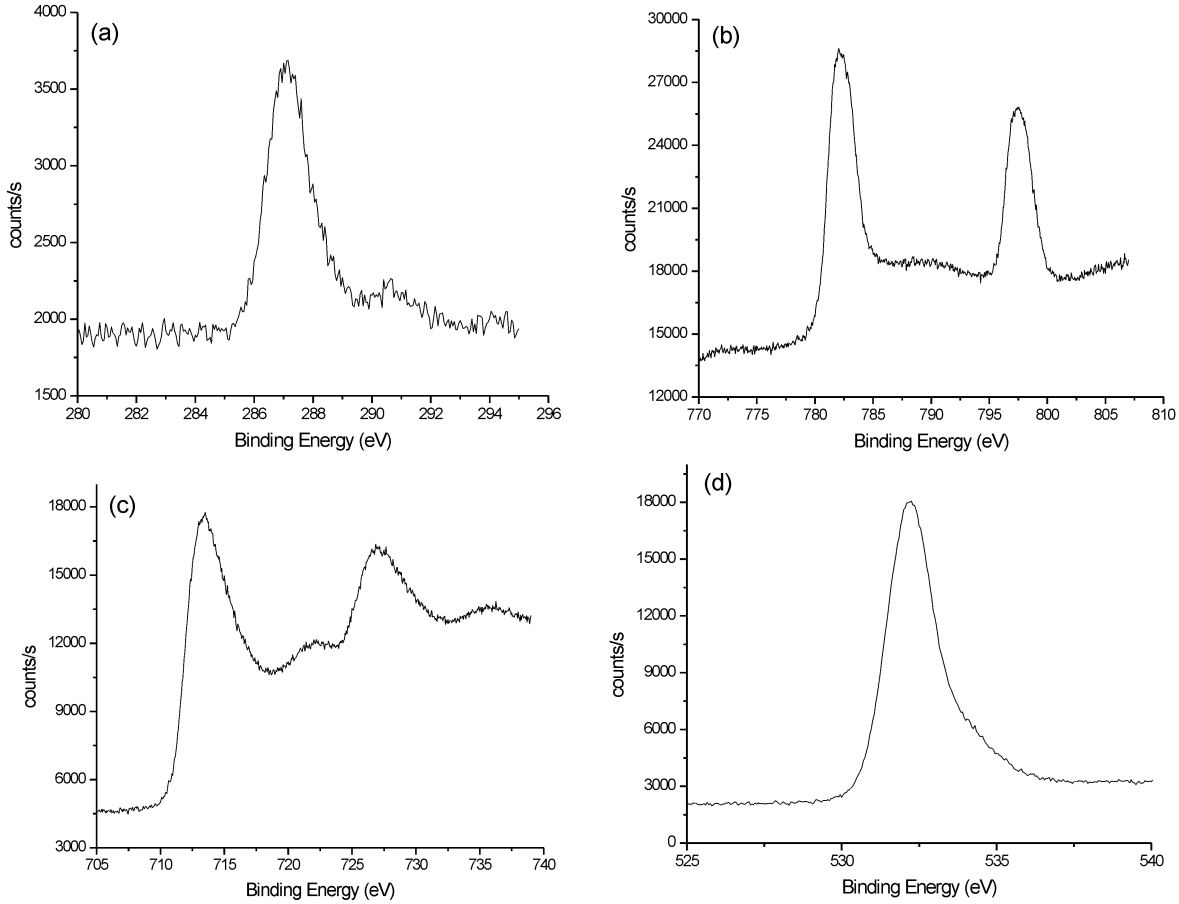

Figure 3. Results of electron spectroscopy for chemical analysis of heat-treated BfC12. The peaks shown are for (**a**) carbon, (**b**) barium, (**c**) iron and (**d**) oxygen atoms.

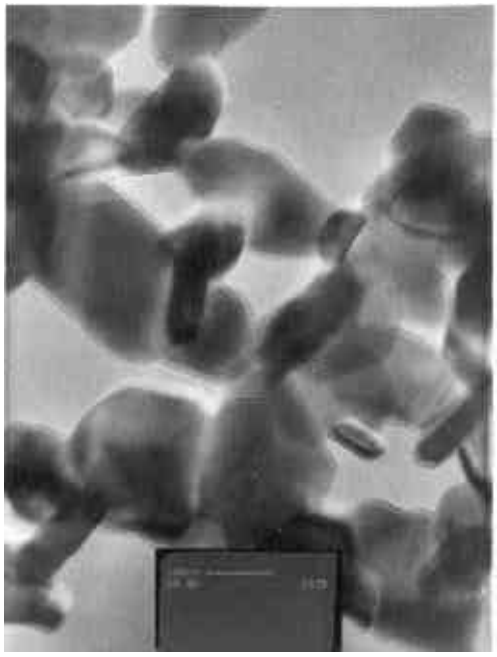

Figure 4. TEM photograph of BfP7C12 showing hexagonal morphology (scale: 100 nm).

The concentration of each element is estimated in atomic percent using the normalized area under the peaks and the ratio is as expected stoichiometrically.

Finally, the carbon contents are analysed to determine the amount of carbonaceous species present in the sample. The XPS data shown in figure 3b reveal that the carbon present in the sample is very little, approximately 1·1 atomic percent. This could also be due to the impurities. This residual carbon has no adverse effect on the properties of the sample. It could, on the contrary, improve the hard magnetic properties if it works as a pinning centres. It is remarkable that monophasic $BaFe_{12}O_{19}$ is synthesized at a low temperature considering that a major peak between 400° and 430°C is observed by the DTA of the pre-fired powder. This suggests that the precursor nanoparticles generated by the auto combustion process are highly receptive to pyrolysis due to their very large specific surface area and that the thermal decomposition of the precursor occurs quite efficiently in air.

Table 1. Magnetic properties of barium ferrite sample synthesized at pH 7.

Fuel ratios	Magnetization (emu/gram)	*Mr* (emu/gram)	M_r/M_s	*Hc* (Oe)	$(BH)_{max}$ (10^6 GOe)
Bf11	46	24	0·52	2587	0·517
Bf12	55	28	0·50	5000	1·013
Bf13	43	22	0·51	4445	0·428

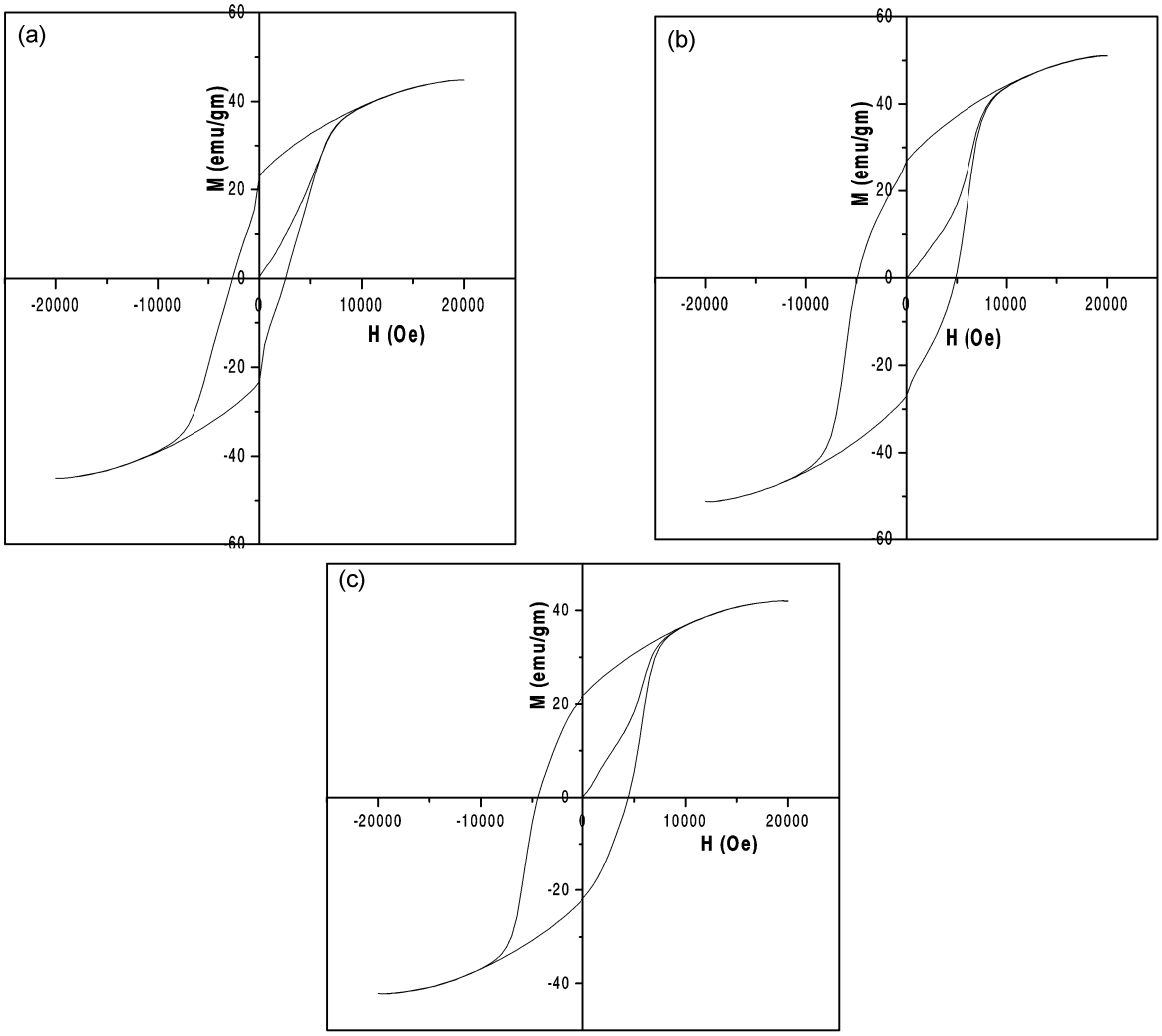

Figure 5. Room temperature hysteresis loop for different samples: (**a**) Bf11, (**b**) Bf12 and (**c**) Bf13.

Particle morphology and size of barium hexaferrite sample recorded by TEM are shown in figure 4 for Bf12 as a typical example. Plates of nearly hexagonal habitus as well as some cylindrical rods are formed. The average particle diameter is between 80 and 100 nm. All samples show crystalline and single-domain particles.

Magnetic behaviour of these barium hexaferrite samples are presented in figure 5. None of the samples show saturation up to a field of 20 kOe. However, they show high remanance and coercivity. Non-saturation may indicate the presence of some fraction of super paramagnetic particles in the sample or an additional phase such as α-Fe_2O_3, which is a canted antiferromagnet. The presence of α-Fe_2O_3 is evident in the XRD pattern of sample Bf13. Its presence in smaller amounts in the other two samples is not ruled out. The magnetization values of the samples Bf11 and Bf13 (~43 emu/gram) are lower compared to the sample Bf12 (~55 emu/gram). The

value obtained is shown in table 1. The reported values of M_s for a monophasic $BaFe_{12}O_{19}$ sample are 53 emu/g,[25] 57·8 emu/g[26] and 61·6 emu/g.[25] The low magnetization values for Bf11 and Bf13 samples could be the consequence of the wide particle size distribution, where there is a small fraction of super-paramagnetic particles contributing to reduce magnetization. The presence of α-Fe_2O_3, which is a canted antiferromagnet, may contribute to the reduction in magnetization value. The squareness ratio (M_r/M_s) is found to be around 0.5 for all three cases which is the expected value for randomly packed single-domain particles.[27] The energy products $(BH)_{max}$ of the samples prepared at fuel ratios 1 : 1, 1 : 2 and 1 : 3 are 0·517, 1·013 and 0·428 MGOe respectively. The maximum energy product $(BH)_{max}$ value was obtained by maintaining fuel ratio at 1 : 2.

We also carried out electron spin resonance (ESR) studies of the samples. In figure 6, we show a typical ESR spectrum of the sample Bf12. The line width ÄH and symmetric resonance absorption can be ascribed to the ferrimagnetic resonance exhibited by Fe^{3+} cations in $BaFe_{12}0_{19}$ at different interstitial sites that couple anti-ferromagnetically due to a super-exchange interaction.[28] Table 2 summarizes these results.

The variation in ÄH can be discussed in terms of anisotropy factors. The distortion of the crystal lattice and the Fe-sites within the lattice contribute their effects to the H_b and H_a anisotropy factors respectively. Theory relevant to ESR has already been discussed elsewhere.[29] Following the results of Shirk and Buessem[30] on $BaFe_{12}O_{19}$, particles of the size and morphology considered here can be characterized by a shape anisotropy $H_b = 4\pi M_s$ (platelets magnetized perpendicular to the plane).

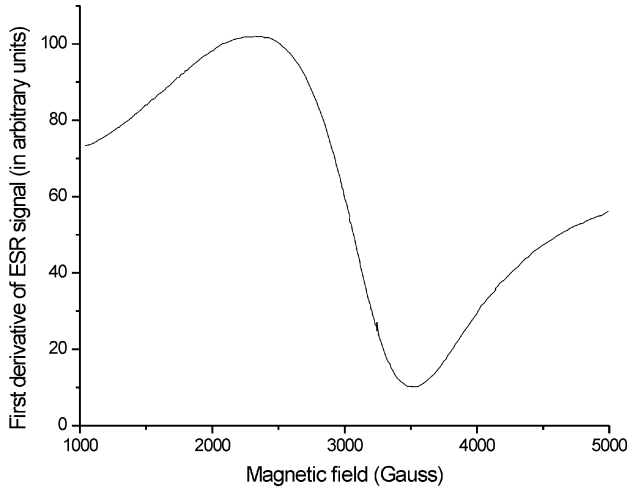

Figure 6. ESR spectra for the sample Bf12 measured at room temperature.

Table 2. ESR parameters of barium ferrite at room temperature.

Fuel ratios	ÄH (gauss)	g factor
Bf11	1000	2·079
Bf12	1050	2·148
Bf13	1700	1·586

Magnetic anisotropy, i.e. due to domain structure (H_d), contributes to ΔH for the sintered samples. The origin and effects of these anisotropies are discussed elsewhere.[31,32] ΔH is also influenced by porosity, eddy currents and inhomogeneous magnetization.[33,34] These factors do not vary much in the samples studied in this investigation. They do, of course, change ΔH by a constant factor (included in ΔH_0 defined below) and effectively do not impart the variation of ΔH for the different samples. Thus we can express ΔH in terms of variation in the anisotropy factors as follows,

$$\Delta H = \Delta H_0 + A\Delta H_a + B\Delta H_b + CH_d, \quad (1)$$

where A, B and C are constants that correlate changes in the respective anisotropy factors to the ΔH. Equation (1) successfully explains the variation in ΔH for the sample series, for the constants $A = B = ½$(assumed empirically),[30] and $H_d = 0$. The H_a and H_b in these samples vary basically owing to the variation in M_s.

It is to be noted that citric acid with one hydroxyl and three carboxyl groups is a multidentate ligand and complexes with multivalent atoms to form chelates. Yu and Huang[14] have suggested that increasing citric acid contents causes more citric acid to ionize, resulting in more carboxylic groups (COOH) chelating with Fe^{3+} and Ba^{2+} in the solution. It is believed that the high degree of chelation of the metallic ions in the solution is responsible for high uniformity of metallic constituents. Upon heating, the uniformly distributed Fe^{3+} and Ba^{2+} can convert to hexagonal barium ferrite more easily and completely. That partially explains the better magnetic properties of the sample Bf12 as compared to Bf11. But we also observe a deterioration in the properties of Bf13. This is because of the presence of α-Fe_2O_3 phase. It is suggested that as the ratio increases beyond an optimum level, the exothermicity of the reaction due to excess citric acid promotes formation of secondary

phases and brings about deterioration of the magnetic properties.

4. Conclusion

It can be concluded that crystalline and single-domain barium ferrite can be synthesized through sol–gel auto combustion technique with citric acid as a fuel at pH 7. In the present work, barium ferrite synthesized at 1 : 2 ratio of cations to citric acid exhibits better magnetic properties. Higher magnetic moment (55 emu/g), high coercivity value (5000 Oe) and maximum energy product $(BH)_{max}$ ($1{\cdot}013 \times 10^6$ GOe) are obtained at 1 : 2 fuel ratios. A large increase in ESR line width has been observed for citric acid ratio 1 : 3. An explanation based on anisotropy and spin relaxation time has been provided which confirms the magnetic results.

References

1. Fujiwara T, Isshiki M, Suzuki T, Ito T and Ido T 1985 *IEEE Trans. Magn.* **21** 1480
2. Candac T S, Carpenter E E, O'Connor C J, John V T and Li S 1998 *IEEE Trans. Magn.* **34** 1111
3. Pillai V, Kumar P, Hou M J, Ayyub P and Shah D O 1995 *Adv. Coll. Int. Sci.* **55** 241
4. Wiley B, Sun Y, Chen J, Hu Cang, Li Z Y, Li X and Xia Y 2005 *MRS Bull*. **30** 356
5. Pileni M P, Ninham B W, Kryzwicki T G, Lisiecki J T I and Filankembo A 1999 *Adv. Mater.* **11** 1358
6. Murphy C J and Jana N R 2002 *Adv. Mater.* **14** 80
7. Patil K C, Aruna S T and Mimani T 2002 *Curr. Op. Solid State Mater. Sci.* **6** 507
8. Choi H J, Lee K M and Lee J G 2001 *J. Power Sources* **103** 154
9. Shikao S and Jiye W 2001 *J. Alloys and Compounds* **327** 82
10. Julien C, Lopez M A C, Mohan T, Chitra S, Kalyani P and Gopukumar S 2000 *Solid State Ionics* **135** 241
11. Castro S, Gayoso M, Rivas J, Greneche J M, Mira J and Rodriguez C 1996 *J. Magn. Magn. Mater*. **152** 61
12. Aruna S T and Patil K C 1998 *Nano Structr. Mater*. **10** 955
13. Chick L A, Pederson L R, Maupin G D, Bates J L, Thomas L E and Exarhos G J 1990 *Mater. Lett*. **10** 6
14. Yu H F and Huang K C 2003 *J. Magn. Magn. Mater*. **260** 455
15. Purohit R D, Tyagi A K, Mathews M D and Saha S 2000 *J. Nucl. Mater.* **280** 51
16. Fraigi L B, Lamas D G and Walsoe de Reca N E 2001 *Mater. Lett.* **47** 262
17. Janasi S R, Emura M, Landgraf F J G and Rodrigues D 2002 *J. Magn. Mater*. **238** 168
18. Carp O, Barjega R, Segal E and Brezeanu M 1998 *Acta Mater*. **318** 57
19. Affleck L, Auguas M D and Parkin I P 2000 *J. Mater. Chem.* **10** 1925
20. Huang J, Zhuang H and Li W 2003 *Mater. Res. Bull*. **38** 149
21. Wagner C D, Riggs W M, Davis C E and Moulder J F 1978 *Handbook of X-ray photoelectron spectroscopy* (ed.) G E Muilenberg (Perkin Elmer Corp)
22. Bera S, Prince A A M, Velmurugan S, Ranganathan P S, Gopalan R, Paneerselvam G and Narasimhan S V 2001 *J. Mater. Sci*. **36** 5379
23. Allen G C and Hallam K R 1996 *Appl. Surf. Sci.* **93** 25
24. Allen G C, Harris S J, Jutson J A and Dyke J M 1989 *Appl. Surf. Sci.* **37** 111
25. Yu H F and Huang K C 2003 *J. Magn. Magn. Mater*. **260** 455
26. An S Y, Lee S W, Lee S W and Kim C S 2002 *J. Magn. Magn. Mater.* **242** 413
27. Benito G, Morales M P, Requena J, Raposa V, Vazquez M and Moya J S 2001 *J. Magn. Magn. Mater.* **234** 65
28. Smit J and Wijn H P J 1959 *Ferrites* (New York: John Wiley)
29. Misra S K, Rane M V, Srivastava C M and Bahadur D 1998 *J. Magn. Magn. Mater*. **187** 93
30. Shirk B T and Buessem W R 1970 *J. Am. Ceram. Soc*. **53** 192
31. Bahadur D, Kollali S, Rao C N R, Patni M J and Srivastava C M 1979 *J. Phys. Chem. Solids* **40** 981
32. Griseom D L 1980 *J. Non-Cryst. Solids* **42** 287
33. Sparks M 1965 *J. Appl. Phys.* **36** 1570
34. Srivastava C M and Patni M J 1974 *J. Magn. Res.* **5** 359